BRAIN
ORIGINAL ARTICLE

Boosting hemianopia recovery: the power of interareal cross-frequency brain stimulation

Estelle Raffin,[1,2,†] Michele Bevilacqua,[1,2,†] Fabienne Windel,[1,2] Pauline Menoud,[1,2] Roberto F. Salamanca-Giron,[1,2] Sarah Feroldi,[1,3] Sarah B. Zandvliet,[1,2] Nicola Ramdass,[1] Laurijn Draaisma,[1,2] Patrik Vuilleumier,[4] Adrian G. Guggisberg,[5,6] Christophe Bonvin,[7] Lisa Fleury,[1,2] Krystel R. Huxlin,[8] Elena Beanato[1,2] and Friedhelm C. Hummel[1,2,9]

[†]These authors contributed equally to this work.

Visual field loss is a common consequence of stroke and manifests in approximatively one-third of patients in the chronic stage. Such loss can significantly impact daily life activities, compromising tasks such as reading, navigating or driving. Although slow and labour intensive, evidence suggests that early interventions with tailored rehabilitation programmes might stimulate visual recovery and improve quality of life in stroke survivors.

To enhance the effects of such rehabilitation programmes, we designed a novel, non-invasive, pathway-specific, physiology-inspired cross-frequency brain stimulation protocol, where complex oscillatory signal integration was inferred from phase–amplitude coupling of oscillatory signals between the primary visual cortex and the motion-sensitive medio-temporal area. Sixteen stroke patients were enrolled in a double-blind, randomized, cross-over trial, during which they performed two blocks of 10 daily training sessions of a direction discrimination task, combined with one of the two cross-frequency transcranial alternative brain stimulation (cf-tACS versus control cf-tACS) conditions.

We found that the cf-tACS condition promoting feedforward visual inputs to the medio-temporal area significantly enhanced motion discrimination performance and shifted visual field borders (i.e. through localized enlargement of isopters). Behavioural improvements associated with a change in oscillatory activity within motion processing pathways were proportional to the amount of residual structural fibres along these pathways and perilesional primary visual cortex activity. In sum, we report, for the first time, that cf-tACS, a novel, pathway-specific, physiology-inspired brain stimulation approach, is able to boost the efficacy of perceptual training, restoring visual motion processing and reducing the severity of visual impairments in adult stroke patients.

1 Defitech Chair of Clinical Neuroengineering, Neuro-X Institute, École Polytechnique Fédérale de Lausanne, Geneva 1202, Switzerland
2 Defitech Chair of Clinical Neuroengineering, Neuro-X Institute, EPFL Valais, Clinique Romande de Réadaptation, Sion 1950, Switzerland
3 School of Medicine and Surgery, University of Milano-Bicocca, Monza 20052, Italy
4 Laboratory of Neurology and Imaging of Cognition, Department of Fundamental Neurosciences, University Geneva, Geneva 1205, Switzerland
5 Department of Clinical Neuroscience, University Hospital of Geneva Medical School, Geneva 1201, Switzerland
6 Department of Neurology, University Hospital of Berne, Inselspital, Berne 3010, Switzerland
7 Stroke Unit Valais, Hôpital du Valais, Sion 1951, Switzerland
8 The Flaum Eye Institute and Center for Visual Science, University of Rochester, Rochester, NY 14620, USA
9 Department of Clinical Neuroscience, University of Geneva Medical School, Geneva 1206, Switzerland

Received February 07, 2025. Revised May 14, 2025. Accepted June 18, 2025. Advance access publication November 17, 2025

Correspondence to: Estelle Raffin
Defitech Chair of Clinical Neuroengineering
Neuro-X Institute (INX), Swiss Federal Institute of Technology (EPFL)
Campus Biotech, Geneva 1202, Switzerland
CNRS and LPNC, Univ. Grenoble Alpes, 38056 Grenoble, France
E-mail: estelle.raffin@univ-grenoble-alpes.fr

Correspondence may also be addressed to: Friedhelm C. Hummel
Defitech Chair of Clinical NeuroengineeringNeuro-X Institute, École Polytechnique Fédérale de Lausanne
1202 Geneva, Switzerland
E-mail: friedhelm.hummel@epfl.ch

Keywords: visual recovery; cross-frequency interactions; interareal synchronization; bifocal transcranial alternating current stimulation; motion direction discrimination

Introduction

Visual field loss manifests in about one-third of stroke patients.[1,2] Among the various forms of visual field defects, homonymous hemianopia is the most common form. It involves a loss of vision in the same half of the visual field through both eyes after unilateral retrochiasmal lesions (i.e. involving the optic tract, the lateral geniculate nucleus, the optic radiations and/or the occipital cortex).[3] Visual field deficits are associated with a myriad of functional impairments in reading, navigation and driving a car, among others,[4,5] significantly decreasing quality of life.[6,7] Despite the increasing demand arising from an ageing population, there is currently no accepted therapeutic solution. The main clinical options are compensatory in nature rather than restorative, implying that they do not induce any significant reversal or restitution of visual deficits caused by the stroke.[8-10]

One main factor that contributes to the lack of established treatment for homonymous hemianopia comes from early descriptive studies that showed limited spontaneous recovery, with stabilization of visual field deficits after 6 months post-stroke.[11-13] This led to the postulate that the visual system had poor capacities for functional recovery. However, there is encouraging evidence to indicate that highly intensive, visual-attentional training protocols presented within the parametrically defined scotoma or blind field might lead to localized improvements in vision.[14-19] Nevertheless, these protocols typically require months of training with intensive patient commitment, and they seem to provide only a moderate amount of improvement that is transferable to everyday life.[14,16,20,21] Targeted interventions inspired from brain physiology, in particular circuit-level synchronization of neuronal oscillations within the visual pathways, might enhance visual training effects and recovery after stroke.

Neural oscillations are considered essential for the dynamic coordination of brain circuits and systems.[22] These oscillations, occurring at specific frequencies, reflect the temporal synchronization of neuronal population activity and can be detected through spiking time series, multi-unit activity, local field potentials, but also using non-invasive methods, such as magnetoencephalogram and EEG. A key breakthrough in past decades has been the discovery of higher-order interactions implemented by oscillatory activity at different frequencies that interact through cross-frequency coupling.[23-25] For instance, the intricate and intertwined oscillatory activity involved in visual processing has been studied extensively.[26-28] This activity reflects the coactivation of millions of neurons, creating distinct oscillatory channels that transmit information across brain regions. Electrocorticography recordings have shown that interareal interactions, mediated by cross-frequency coupling, increase along the visual hierarchy, potentially enhancing the processing of spatially predictable targets.[26,29] More precisely, studies have consistently documented temporally segmented ongoing gamma-band activity (>40 Hz), synchronized with distinct phases of alpha-band activity (8–13 Hz) in the visual cortex of cats, monkeys[30,31] and humans.[32-34] This synchronization mode enables efficient gating and filtering of sensory information. This is particularly relevant for visual retraining protocols, where a strong anticipatory processing of spatial attention is expected.[20]

Building on an improved understanding of circuit interactions between visual areas during motion stimulus processing, we designed a non-invasive, pathway-specific, cross-frequency brain stimulation protocol to enhance interareal interactions.[35] In this context, low-frequency oscillations provide a temporal structure that modulates high frequency-based local processing. Hence, non-invasive injection of synchronized alpha oscillations into the primary visual cortex (V1) onto gamma oscillations in the motion-sensitive mediotemporal area (MT)[36] by means of cross-frequency transcranial alternating current stimulation (cf-tACS) provides experimental conditions that can promote bottom-up direction of information flow. A single session of this cf-tACS condition has been shown to increase V1 alpha–MT gamma coupling in healthy young participants and in stroke patients.[35] Combined with an established visual retraining protocol involving the presentation of moving dots immediately inside the border area of the scotoma,[16,19,20] we asked whether strengthening these specific, coordinated oscillatory motifs is able to reinstate more 'physiological' interareal interactions and whether this is associated with an improvement in global motion direction perception when paired with a random dot stimulus during training. We also examined whether perceptual learning transferred into improved luminance detection at trained blind-field locations. Finally, unique multimodal data that included EEG recordings, functional MRI (fMRI) and structural MRI were acquired in each participant to decipher the underlying mechanisms of pathway-specific cross-frequency tACS for visual field recovery, with a special focus on the integrity and efficiency of the V1–MT pathway.

Materials and methods

Patients

Sixteen adult patients were enrolled ≥1 week after stroke-induced occipital damage (verified using structural MRIs), with reliable 30-2 Humphrey visual field perimetry in both eyes and the ability to

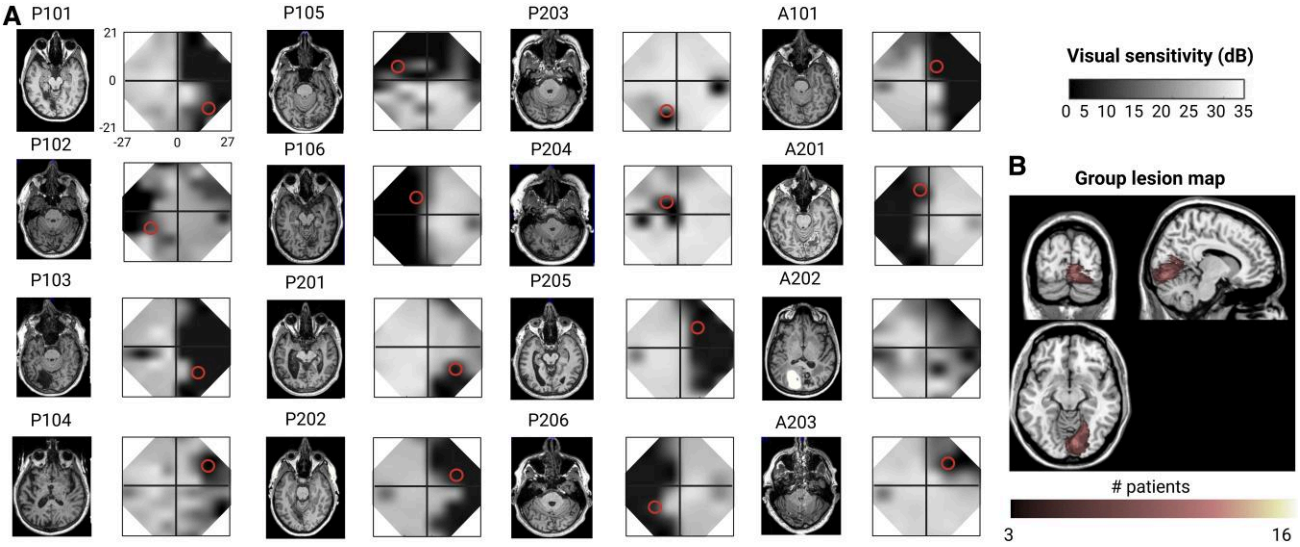

Figure 1 Initial visual field deficit and lesions map. (**A**) Composite visual field maps derived from Humphrey perimetry showing the initial loss of conscious luminance detection sensitivity and T1 Magnetization Prepared Rapid Gradient Echo (MPRAGE) images of all individual patients. Red open circles indicate the location and size of visual stimuli used for training. Note that Patient A202 dropped out after the baseline assessments. (**B**) Lesion overlay maps are mirrored to the right hemisphere when needed.

Table 1 Patients' characteristics and demographics

ID	Age (years)	Sex	Lesion	Lesion side	Time since stroke (months)	MMSE
P101	34	Female	Cort	Left	12	27
P102	62	Male	Cort	Right	12	28
P103	74	Male	Cort	Left	60	25
P104	62	Male	Cort	Right	12	27
P105	66	Male	Cort + subcort	Right	30	27
P106	68	Male	Cort	Right	8	29
P107	53	Male	Cort	Left	2	30
P201	69	Male	Cort + subcort	Left	28	25
P202	40	Female	Cort	Left	11	28
P203	59	Male	Cort	Right	4	28
P204	63	Male	Cort	Right	4	29
P205	51	Male	Cort	Left	3	30
P206	56	Male	Cort	Right	11	30
A201	55	Male	Cort	Right	1	29
A202	78	Female	Cort	Left	1	21
A203	66	Male	Cort	Left	1.5	29

Note that all patients had a cortical lesion (Cort) restricted to the primary visual cortex, except P104 and P201, who had a primary visual cortex lesion and a subcortical lesion (subcort) affecting the left putamen and the right posterior thalamus, respectively. MMSE = Mini-Mental State Examination.

fixate precisely (error smaller than ±1° relative to fixation spot) during psychophysical testing. The median time since stroke was 11 months (range: 1–60 months). Exclusion criteria were unreliable Humphrey visual fields, neglect, neurological disease unrelated to occipital stroke, use of neuroactive drugs, and any contra-indication to MRI or non-invasive brain stimulation. Seven patients had left-sided homonymous visual field loss and nine had right-sided homonymous visual field loss. Twelve patients had homonymous hemianopia and four had homonymous quadrantanopia (Fig. 1A). Mean (standard deviation) age was 59.93 (11.2) years, range 34–74 years; 18.75% were female and 81.25% male; in all patients but one, the aetiology of brain injury, as verified by cranial CT and/or MRI, was an infarction in the territory of the posterior cerebral artery causing a lesion to the occipital cortex; one patient had a carotid artery rupture. Note that all but one patient had an ipsilesional MT left intact by the lesion (for the lesion overlay map, see Fig. 1B). None of the patients had received or were receiving any treatment for their visual field defect at the time of the study. All patients were native French speakers except for one German patient, and all had ≥5 years of education (see Table 1).

Study design

Patients were randomly allocated to one of two treatment groups: Group A ($n = 8$) first received forward cf-tACS followed by backward cf-tACS, whereas Group B ($n = 8$) first received backward cf-tACS followed by forward cf-tACS in a cross-over design (Fig. 2A). Each block consisted of 10 consecutive sessions (excluding weekends) of backward or forward cf-tACS applied over 15 days, concurrently with training on a left–right direction discrimination and integration (CDDI) task at a selected, blind-field location (red circles in Fig. 1A). The two blocks were performed ≥1 month apart. Before

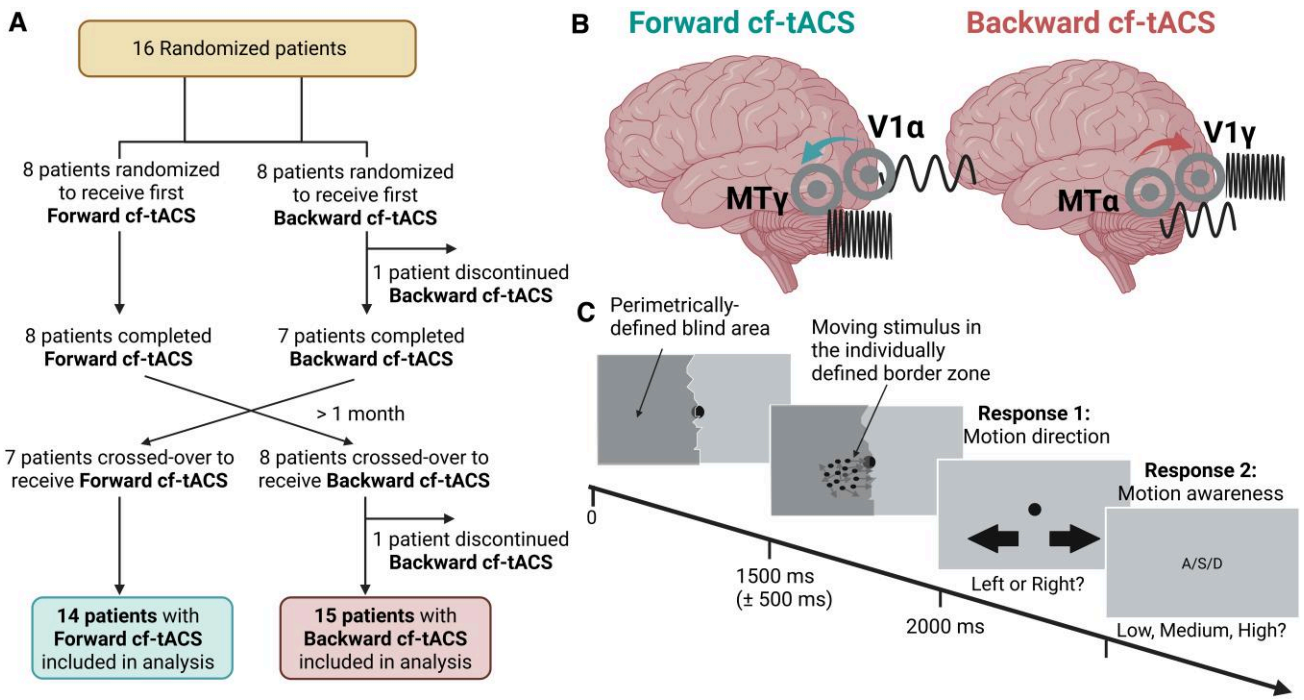

Figure 2 Study design, cf-tACS interventions and visual training task. (**A**) Study flow diagram. (**B**) Schematic representation of the two interventions: forward cf-tACS and backward cf-tACS. (**C**) Coarse Direction Discrimination and Integration (CDDI) task illustration. cf-tACS = cross-frequency transcranial alternating current stimulation.

and after each block, patients performed a 24-2 Humphrey visual field perimetry test, clinical scales, EEG and MRI recordings.

This study belongs to a registered trial (ClinicalTrials.gov: NCT05220449), was approved by the local Swiss Ethics Committee (2017-01761) and was performed within of the guidelines of the Declaration of Helsinki.

Backward and forward cf-tACS

Two customized centre–surround electrodes (outer and inner diameters: 5 and 1.5 cm, respectively) were connected to two Neuroconn DC Plus stimulators (Neurocare), which were triggered repetitively and at the same time to ensure no time lag between the two signals. The International 10/20 system was used for the localization of V1 (O2 or O1 for the left or right hemisphere, respectively) and MT (PO8 or PO7 for the right and left hemisphere, respectively) on the lesioned hemisphere. A constant current intensity of 3 mA was applied in both stimulators, creating a current density of 0.18 mA/cm^2. An *a priori* defined individual α [8–12 Hz] and γ [30–45 Hz] peak frequencies were used to apply tACS. The peak frequencies were extracted from a 5 min resting-state EEG prior the intervention. Forward tACS refers to V1 α–MT γ tACS, and backward tACS corresponds to V1 γ–MT α tACS (Fig. 2B). Each tACS session lasted ∼30 min and was administered at the same hour every day.

Training task

During tACS, patients performed a Coarse Direction Discrimination and Integration (CDDI) task involving a random dot stimulus appearing for 500 ms in a 5°-diameter circular aperture displayed on a computer screen (1024 × 768 at 144 Hz frame rate) (Fig. 2C). The stimulus consisted of black dots moving on a mid-grey background (dot lifetime: 250 ms, speed: 5°/s, density: 3.5 dots/°^{2}). Dots moved globally in a range of directions distributed uniformly around the leftward or rightward vectors.[16,20,37] Participants had to respond whether the global direction of motion was left- or rightward. Task difficulty was adjusted using a 3:1 staircase, increasing dot direction range from 0° to 360° in 40° steps. Training sessions consisted of 255 trials. The visual stimulus location was individually defined as followed: after Humphrey perimetry, each subject underwent extensive psychophysical mapping of the blind-field border, as previously described.[16,20] Training location was selected as the location where performances on the CDDI task declined to chance level (50%–60% correct) upon a small movement from the intact hemifield into the Humphrey-defined blind field. All training sessions were performed inside a shielded EEG room equipped with a Windows machine running MATLAB (Mathworks Inc., USA) and Psychtoolbox, an EyeLink 1000 Plus Eye Tracking System (SR Research Ltd, Canada) and a chin rest. Individuals sat at 60 cm from the computer screen, supporting their heads with the chin rest, while fixation during all trials was controlled with the eye tracker. If gaze shifted by >1° from the fixation spot, the trial was discarded and replaced.

Direction range thresholds

Daily task performance was fitted using a Weibull psychometric function, with a threshold criterion of 72% correct used to calculate direction range thresholds, where percentage correct = 1 – (1 – chance) × exp[– (*k* * x/threshold) slope] and *k* = {–196 log[(1 – 0.72)/(1 – chance)]}$^{(1/slope)}$.

Both direction range and direction range thresholds were normalized to the maximum range of directions in which dots could move (360°) and expressed as a percentage using the following formula: normalized direction range (NDR, as a percentage) = (360° – direction range threshold)/360° × 100. For ease of analysis, when participants performed at chance (50%–60% correct for a given session), the NDR threshold was set to 100%.

Perimetric mapping of visual field defects

Perimetry was conducted using a Humphrey Field Analyzer II-i750 (Zeiss Humphrey Systems, Carl Zeiss Meditec) and MonCvONE-SAP (Metrovision) by a scientist blinded to the group allocation of each participant. The static 30-2 testing patterns were collected for each eye, repeated twice with a break in between. Sensitivity thresholds were determined at a specified number of test locations, with fixation controlled using the systems' eye tracker and gaze/blind spot automated controls, visual acuity corrected to 20/20, a white size III stimulus, and a background luminance of 11.3 cd/m^2.

To refine scotoma boundaries, we additionally performed kinetic perimetry using the same perimeters mentioned above that emulates manual standard Goldmann perimetry[38] twice on each eye, whereby sensitivity thresholds were determined by moving stimuli of various sizes and light intensities along a vector from the blind region to a seeing region. Stimulus speed was 4°/s, the visual field size was 30° with a grid resolution of 5°, a white size III stimulus was used, with a background luminance of 11.3 cd/m^2. This measures the concentric constriction of the isopter. This returns contour lines or isopters with a very high spatial resolution, resulting in a map of visual field sensitivity.[39] Measurements were performed either at the Centre Medical Universitaire (CMU) in Geneva or at the Clinique Romande de Réadaptation in Sion, by the same operators.

Luminance detection thresholds obtained from the four static test patterns were averaged from identical locations in the two eyes to produce a unique visual map and interpolated in MATLAB (Mathworks) to create one composite static visual field map for each patient, as previously described.[15] For the kinetic perimetry, stopping radial positions for each meridian were averaged and displayed on a polar plot, reflecting visual field borders. From these boundaries, surface maps were computed in degrees squared. To determine potential changes, difference maps were generated; significant areas that improved on the static perimetry were defined as visual field locations that differed by ≥6 dB [conservative standard of change at twice the measurement error of the Humphrey test (Zeiss Humphrey Systems, Carl Zeiss Meditec)].[15] For the kinetic perimetry, a minimum increase of 10°^{2} localized offset compared with the normal isopter (i.e. no defect) is considered to be significant.[40]

EEG recording and analyses

Resting-state EEG and task-EEG activity (using the CDDI task) was recorded before the first session and after the last training session of each block using a 64-channel, transcranial magnetic stimulation (TMS)-compatible, active system (BrainAmp DC amplifiers and BrainCap EEG cap, Brain Products GmbH). The EEG cap set-up was done according to the 10–20 standard system. Electrode impedances were adjusted and kept <10 kΩ using conduction gel. Impedance levels were checked throughout the experiment and corrected if needed during breaks between conditions. The signal was recorded using DC mode, filtered at 500 Hz with an anti-aliasing low-pass filter, and digitalized at 5 kHz sampling frequency. During the experiment, the ground electrode was Fpz, and reference electrode was Cz.

All the preprocessing steps were run in MATLAB, using the EEGLAB toolbox.[41] Data were re-referenced to the average of all channels, band-pass filtered between 1 and 80 Hz, notch filtered between 48 and 52 Hz, and divided into epochs of 1.5 s length. Visual inspection was used to remove explicit artefacts among channels and trials, followed by the reconstruction of dropped channels and epochs. Ultimately, an independent component analysis was applied to the downsampled data (1000 Hz) to remove electrophysiological interferences, such as eyeblinks or muscle artefacts. Brainstorm software[42] together with OpenMEEG BEM plugins were used to perform source-level reconstruction of EEG data. Initially, the cortex and head mesh (15 000 and 10 000 vertices, respectively) of the patient were generated using the automated MRI segmentation routine of FreeSurfer.[43] The forward model was then computed using the symmetric boundary element method developed in the open OpenMEEG freeware, using default values for conductivity and layer thickness.[44] The source-level activation was computed using a minimum norm imaging linear method with sLORETA as inverse model. The dipole orientation of the source model has been defined as constrained to the cortex surface. The covariance matrix was computed from the concatenated epoch baselines, e.g. the recorded activity before the onset of each trial (–0.5 to 0.005 s). All metrics involving a frequency-domain decomposition were calculated through Morlet wavelets between 2 and 60 Hz. The source points belonging to specific areas of interest (i.e. primary visual cortex (V1), motion-sensitive medio-temporal area (MT), intraparietal sulcus, frontal eyed field (FEF)) were defined manually for each subject according to the fMRI localizer recordings performed before the EEG acquisitions.

Initially, we examined the time–frequency content of the V1–MT pathway during the CDDI task at the source level. Given that our tACS interventions were based on the V1–MT phase–amplitude relationship, we computed the two directions of source-based phase–amplitude coupling (PAC)[45] between V1 and MT (i.e. α_{phase} V1 γ_{amp} MT and γ_{amp} V1 α_{phase} MT). This was done using the spectral source activity, with phase data frequency ranging from 8 to 12 Hz and amplitude data ranging from 30 to 45 Hz, by means of the EEGLAB plug-in Event Related PACTools (PACTools).[46] Specifically, PAC was defined as:

$$\mathrm{PAC} = \frac{1}{n} \left| \sum_{t=1}^{n} a_t(f)\, e^{i\theta_t} \right| \quad (1)$$

where t corresponds to a certain time point, a denotes the power at a certain specific frequency for this specific time point, i is the imaginary variable, θ the phase angle and n the number of time points.

MRI recording and analyses

Whole-brain MRI was performed with a 3 T Siemens scanner available at Fondation Campus Biotech Genève (FCBG), Geneva, Switzerland or the same scanner at Hôpital du Valais, Sion, Switzerland. High-resolution anatomical images were acquired for reference using an Magnetization-Prepared Rapid Gradient Echo (MPRAGE inversion time = 900 ms, with voxel size = 1 mm × 1 mm × 1 mm. One run of 657 scans with the measurement of the T2*-weighted blood oxygenation level-dependent (BOLD) effect was acquired with a gradient echo-planar imaging protocol and the following parameters: echo time (TE) = 30 ms, repetition time (TR) = 1000 ms, flip angle = 90°, voxel size = 3 mm × 3 mm × 2 mm, field of view = 204 mm × 204 mm, matrix size = 68 × 68, and 37 axial slices each of 2 mm thickness. Finally, diffusion-weighted MRI data were acquired using a pulsed gradient spin echo sequence with the following parameters: TR = 5000 ms; TE = 77 ms; slices = 84; field of view = 234 mm × 234 mm; voxel resolution = 1.6 mm × 1.6 mm × 1.6 mm; slice thickness of 1.6 mm; readout bandwidth = 1630 Hz/pixels; 64-channel head coil; and GRAPPA acceleration factor = 3. Seven T2-weighted images without diffusion weighting (b0; $b = 0$ s/mm^2) were acquired, including one in the opposite phase encoding direction. A total of 101 images with non-collinear diffusion gradient directions distributed equidistantly over the half-sphere and covering five diffusion-weighting gradient strengths were obtained [b-values = (300, 700, 1000, 2000, 3000) s/mm^2; shell samples = (3, 7, 16, 29, 46)].

Functional MRI

Data were analysed using the Statistical Parametric Mapping toolbox (SPM12b, Wellcome Trust Center, London, UK; http://www.fil.ion.ucl.ac.uk/spm), implemented in MATLAB 2019b (The Mathworks Inc., MA, USA). The preprocessing steps included correction for field inhomogeneity, slice timing correction, motion correction and unwarping. Then, the structural image of each participant was co-registered to the mean realigned echo-planar imaging (EPI) volume. The co-registered T1 image was then normalized to the Montreal Neurological Institute (MNI) reference space using the unified segmentation approach.[47] The resulting deformation parameters were applied to the individual EPI volumes, which were then smoothed using an isotropic 4 mm full-width half-maximum Gaussian kernel.

For all datasets, we modelled a General Linear Model using two regressors based on the subject's trial-by-trial accuracy in line with our staircase procedure {correct [74.63 (±9.6) trials/incorrect (25.99 (±9.7) trials]}. Regressors were modelled as series of events (representing individual epochs) convolved with a canonical haemodynamic reference waveform. Low-frequency confounds were controlled by high-pass filtering at 1/128 Hz, and head-movement estimates derived from the realignment procedure served as additional covariates of non-interest. Voxel-wise parameter estimates for all conditions and each covariate resulting from the least mean squares fit of the model to the data were computed. For the group analysis, left-side lesions were mirrored to the right hemisphere. A full factorial design was used with the factors time (pre, post) and tACS condition (forward cf-tACS, backward cf-tACS). *Post hoc* comparisons were performed by extracting beta weights in the significant group-level cluster at the individual level, when significance was reached. The statistical significance threshold was set to a height threshold of $P < 0.001$ uncorrected at the voxel level, and $P < 0.05$ at the cluster level after false-discovery rate correction.

To probe the functional state of the perilesional area and investigate how stimulation of the perilesional area propagates to the rest of the brain, we used online TMS–fMRI coupling.[48] The methodological details regarding TMS–fMRI data acquisition and analyses can be found in the Supplementary material.

Diffusion-weighted imaging

Structural diffusion images were preprocessed by means of FSL[49] and MRtrix[50] software. A denoising step was applied initially via the dwidenoise function (MRtrix), followed by correction of the Gibbs ringing artefact via mrdegibbs (MRtrix).[51] Images were then corrected for motion, susceptibility-induced fields, eddy current-induced distortions, and bias field via the FSL functions topup,[52] eddy_openmp[53,54] and fast.[55] Probability maps for CSF, grey and white matter were estimated from the T1-weighted image via the fast function (FSL), then registered to the average b0 image using ANTs.[56] A fibre orientation distribution function was also derived at the voxel level from multi-shell, multi-tissue-constrained spherical deconvolution. It was then used to compute whole-brain probabilistic tractography via a second-order integration over fibre orientation distribution (iFOD2).[57] The algorithm stopped once 10 million streamlines were generated. Each streamline was then weighted based on spherical deconvolution-informed filtering of tractograms (SIFT2, MRtrix).[58] To extract streamline information between V1, V5 and the thalamus, two main techniques were used. V1 and V5 were derived from the functional localizer using individual, thresholded activation in the ipsi- and contralesional hemispheres. The thalamus was extracted from the Destrieux atlas parcellation, an output of the recon-all function of Freesurfer on the T1-weighted image.[59] All masks were registered to the average b0 image using ANTs. Finally, the function tckedit[50] from MRtrix was used to extract specific streamlines passing through V1 and V5, V1 and the thalamus, or V5 and the thalamus. The sum of the weights or the average fractional anisotropy (FA) along these tracts were used as indicators of cross-sectional area and integrity, respectively.

Statistical analyses

To compare the EEG metrics (phase–amplitude coupling, Granger causality and time–frequency values) before and after the two tACS/training interventions, we used cluster-based non-parametric permutation tests. We evaluated differences in threshold performance for the CDDI task between the two interventions and across days, using a linear mixed model built with the raw NDR threshold as a dependent variable, training day, tACS condition and order as fixed effects, and patient as a random effect. Finally, an ANOVA was applied on the model parameters. When only the two interventions were directly compared without a fixed effect, a paired *t*-test was performed after ensuring normality of the distribution with a Shapiro–Wilk test. Non-parametric equivalents were used if needed. A probability of type I error of $P < 0.05$ was considered statistically significant. Finally, to evaluate the value of a structural and a functional variable for predicting improvements in visual processing after forward cf-tACS, we ran a backward regression model (*P* to enter: 0.05, *P* to remove: 0.1). Change in NDR thresholds was the dependent variable, and the predictors were the lesion sizes, manually extracted from the T1 images of each patients, the activity of perilesional V1 extracted from the combined TMS–fMRI examination and the residual ipsilesional V1–MT tract derived from the diffusion-weighted images.

Results

One patient dropped out after the first block, and one subacute patient was excluded after baseline measurements because of a full spontaneous recovery. As a result, 15 patients completed the forward cf-tACS block and 14 patients completed the backward cf-tACS block.

Forward cf-tACS improves visual function in the blind field

Because the training task relied heavily on motion discrimination, we first examined pre/post changes in kinetic visual field maps. The results revealed that forward tACS significantly improved kinetic visual field boundaries in comparison to backward tACS [forward tACS: $+698.3 \pm 921.8°^2$, backward tACS: $+121.9 \pm 805.3°^2$, paired *t*-test: $t(12) = -2.24$, $P = 0.045$] (Fig. 3A for the group results and pre/post kinetic visual field maps from one example patient). In most patients, the extension corresponded to the trained area (for all kinetic visual field maps, see Supplementary Fig. 1). Baseline maps were not different in the two groups [$t(12) = -0.42$, $P = 0.68$, paired *t*-test]. We also compared the composite visual field maps extracted from static Humphrey perimetry as previously described,[60] before and after the intervention. The static visual field maps showed a significant, localized increase in both conditions, albeit stable visual fields before starting the protocol [Fig. 3B, one-sample *t*-test for forward tACS: $t(13) = 4.33$, $P < 0.001$; for backward tACS: $t(14) = 6.14$, $P < 0.001$; for all individual pre/post differences, see Supplementary Fig. 2]. However, there was no significant difference in static perimetry change between the two tACS conditions [$t(13) = -0.382$, $P = 0.71$, paired *t*-test].

We also measured changes in NDR thresholds, indexing motion perception abilities in the blind field. The performance of patients was close to chance (54.3% ± 4.2% correct) at the beginning of training.

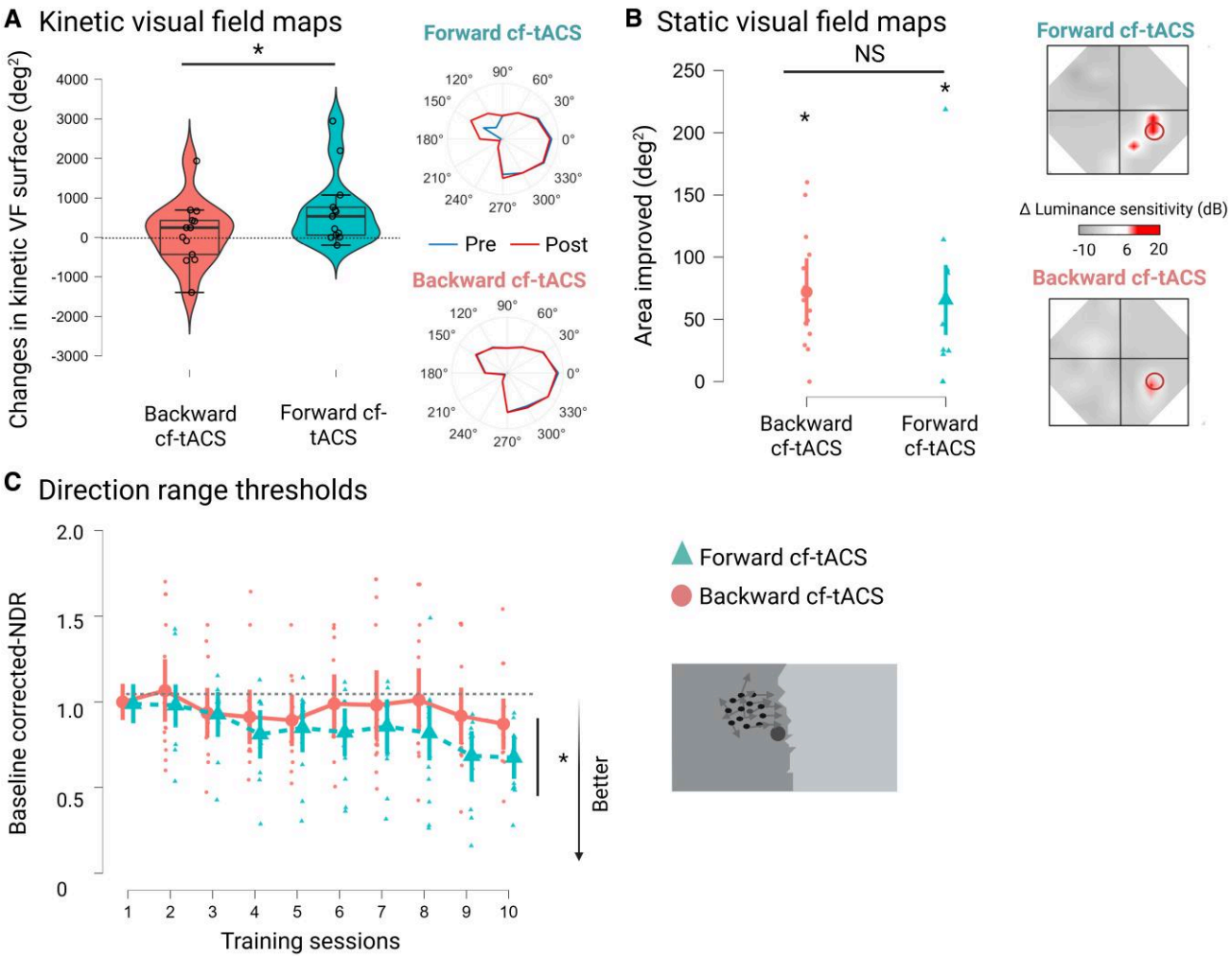

Figure 3 Changes in visual fields and motion direction processing. (**A**) Group difference in kinetic visual field areas between forward cf-tACS and backward cf-tACS. Adjacent maps show kinetic visual field borders of an example patient before (blue lines)/after (red lines) forward cf-tACS and backward cf-tACS, and plots of the area of the Humphrey visual fields that improve by >6 dB[15] after forward cf-tACS and backward cf-tACS (*bottom row*). (**B**) Mean and individual data corresponding to the pre/post improvement in static visual field. (**C**) Baseline-corrected behavioural performance at the training task measured across the 10 daily sessions, for forward cf-tACS and backward cf-tACS. *Significant one-sample *t*-tests in each tACS condition. cf-tACS = cross-frequency transcranial alternating current stimulation.

Importantly, performances at baseline did not differ between forward and backward cf-tACS groups [$t(13) = -1.07$, $P = 0.31$]. Training with both cf-tACS conditions improved NDR thresholds [−19% ± 26%, with respect to baseline; one-sample *t*-test: $t(13) = -4.5$, $P < 0.001$ for forward cf-tACS; and −10.2% ± 31%, one-sample *t*-test: $t(13) = -2.2$, $P = 0.05$ for backward cf-tACS]. The ANOVA testing the mixed linear model on the daily baseline-corrected NDR thresholds showed a significant Training Day × tACS condition interaction [$F(9,196) = 2.5$, $P = 0.01$]. This reflected a dissociation between the two learning curves, observable from Training Day 6, with forward tACS showing larger improvements in motion direction discrimination (Fig. 3C). There was a significant effect of training day [$F(9,27) = 7.14$, $P < 0.001$] but no effect of order or tACS condition ($P > 0.05$). No differences in motion awareness and response times were observed between the two interventions (Supplementary Fig. 3).

Changes in cross-frequency oscillatory coupling

To test the hypothesis that forward cf-tACS would specifically modulate bottom-up V1 α_{phase}–MT γ_{amp} PAC, we compared the maximal PAC values in the time domain during motion processing before and after forward cf-tACS and backward cf-tACS (Fig. 4A , top, with associated co-modulograms provided at bottom).

This analysis revealed an early increase in V1 α_{phase}–MT γ_{amp} PAC at ~100 ms after stimulus onset for forward cf-tACS. This was followed by a significant decrease at ~300 ms after stimulus onset. Interestingly, this pattern of early enhanced bottom-up PAC was already present after only one session of forward cf-tACS (reported in a previous manuscript[61]). The reverse direction, V1 γ_{amp}–MT α_{phase} PAC, showed a significant increase in a late time window at ~300 ms after stimulus onset. Neither of the two PACs showed significant changes after backward cf-tACS.

Changes in functional activity and structural connectivity

To investigate further how motion signals were processed differently after the combined training + cf-tACS intervention, we compared fMRI activation patterns elicited by the same motion

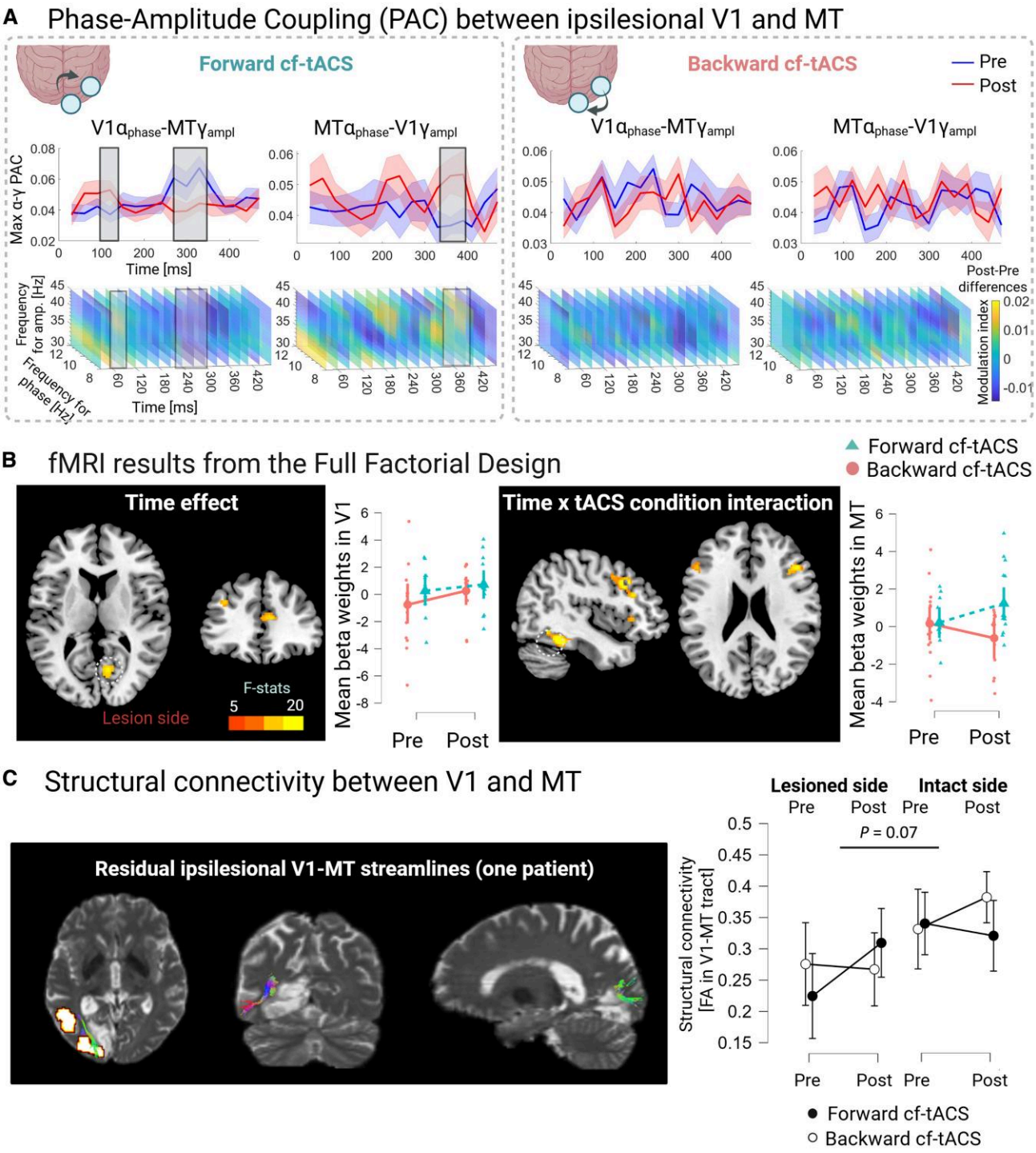

Figure 4 Electrophysiological and imaging results. (**A**) Maximal phase–amplitude coupling between V1 α_{phase}–MT $\gamma_{amplitude}$ and the opposite V1 $\gamma_{amplitude}$–MT α_{phase} for the two tACS groups (*top row*) and the associated co-modulograms (*bottom row*). Significant differences in the phase–amplitude coupling time windows are indicated with grey rectangles. (**B**) Functional MRI results from the full factorial design showing the main effect of time (*left*) with the associated beta weights in V1 for the two tACS conditions. Also shown are the Time × tACS condition interaction, showing significant clusters in the ipsilesional MT, bilateral FEF and ipsilesional lateral prefrontal cortex, and the associated interaction in beta weights in the ipsilesional MT. (**C**) Changes in structural connectivity measured with fractional anisotropy (*left*) and sum of the weighted V1–MT tracts (*right*). No significant differences were found before/after any of the interventions. cf-tACS = cross-frequency transcranial alternating current stimulation; FEF = frontal eye field; MT = medio-temporal area; V1 = primary visual cortex.

discrimination task. We designed a full factorial ANOVA with factors time (pre/post) and tACS condition (forward/backward). This whole-brain analysis led to a significant effect of time in V1. The extracted beta weights in V1 showed a BOLD increase after tACS in both conditions (Fig. 4B). The Time × tACS condition interaction showed significant activity in the ipsilesional MT, bilateral frontal eye field (FEF) and ipsilateral prefrontal cortex (MNI coordinates are reported in Supplementary

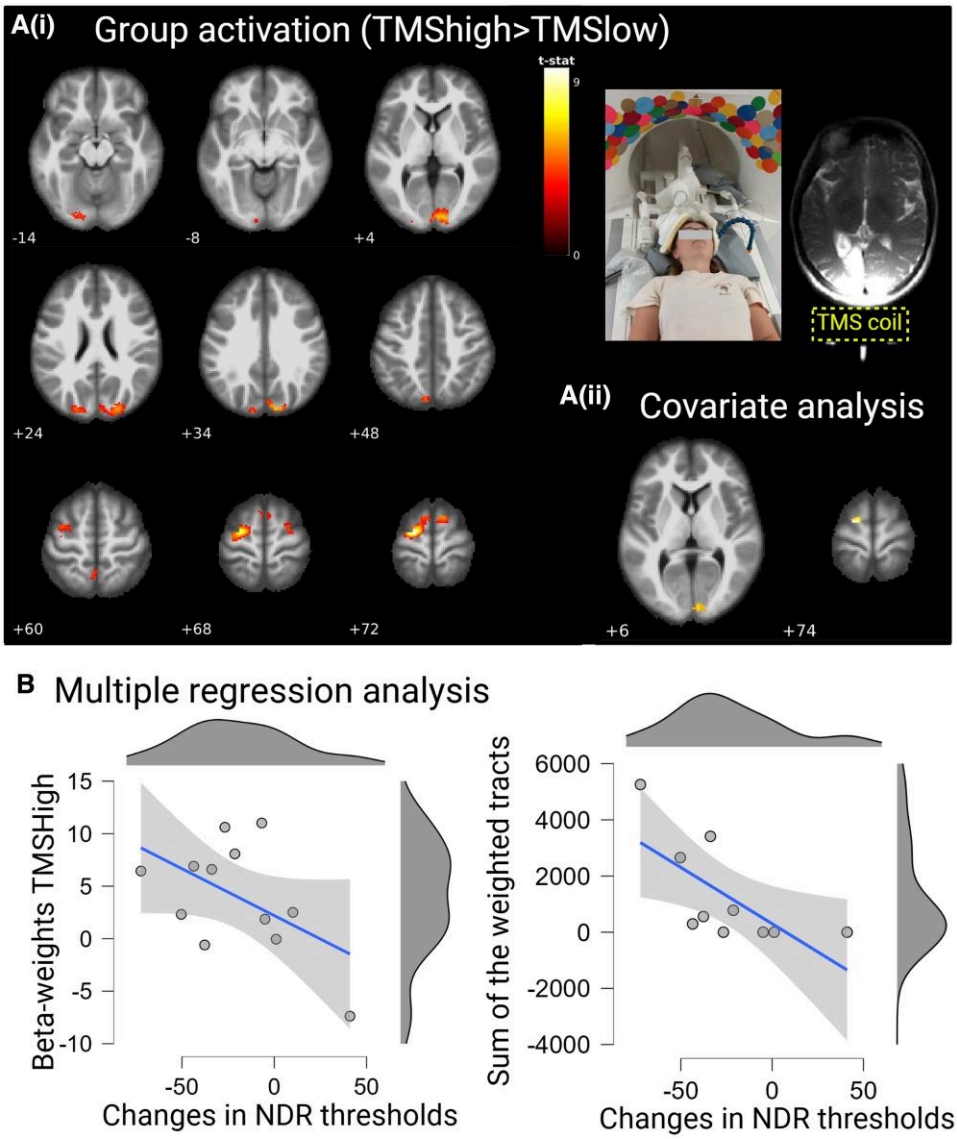

Figure 5 Online TMS–fMRI and regression results. [**A(i)**] Whole group results of the two-sample *t*-test contrasting high-intensity TMS versus low-intensity TMS and TMS–fMRI set-up with the coil positioning. [**A(ii)**] Results of the covariate analysis showing the regions in the ipsilesional V1 and contralesional FEF that increased significantly with improved motion discrimination. (**B**) Regression plots between the normalized detection range (NDR) changes and functional/structural predictors, illustrating the multiple regression analysis. $P < 0.001$ uncorrected, at the voxel level and to that of $P < 0.05$ at the cluster level after false-discovery rate correction. FEF = frontal eye field; MT = medio-temporal area; TMS = transcranial magnetic stimulation; V1 = primary visual cortex.

Table 1). The betaweights in the ipsilateral MT confirmed an increase after forward cf-tACS and a decrease after backward cf-tACS. Note that this contrast also led to a significant cluster in the ipsilesional lateral geniculate nucleus at a more liberal threshold ($P < 0.001$ uncorrected).

We also compared the structural properties of white matter fibres connecting the ipsilesional V1 to the ipsilesional MT using diffusion-weighed imaging, positing that they might underlie the interareal communications reported above. We extracted the sum of the weights and FA of the relevant tracts connecting V1 to MT bihemispherically, reflecting the importance of the bundles and the structural integrity of the tracts, respectively. Although we could not formally detect a significant effect, there was a trend for a side effect, reflecting structural reorganization and loss of structural fibres in the lesioned hemisphere [FA: $F(1,96) = 3.31$, $P = 0.07$] (Fig. 4C).

Baseline functional and structural predictors of forward cf-tACS efficacy

We investigated whether individual functional or structural markers could predict the outcomes of forward cf-tACS in 11 of these patients. One dataset was excluded because of wrong targeting, and four patients did not elect to take part in this optional study. We explored whether substantial residual fibres between V1 and MT or a functionally responsive ipsilesional primary visual cortex is a prerequisite to achieve improvements. We extracted the fMRI-derived beta weights in response to TMS applied to the ipsilesional V1 before the intervention [see Materials and Methods section, Fig. 5A(i) for the TMS–fMRI set-up and Supplementary Fig. 4 for the individual TMS–fMRI set-up for all patient]. Group-wise fMRI activation revealed significant clusters in the perilesional V1 and remote clusters in the bilateral FEF and cuneus (Fig. 4B). To

investigate a potential link between TMS-induced BOLD activity and the individual changes in motion discrimination in the blind field, a covariate analysis was run. It showed a significant activation cluster in the ipsilesional V1 [Fig. 5A(ii)].

Finally, a multiple regression model was built using functional and structural predictors measured prior to the start of the intervention to explain the changes in motion perception: the lesion volume (in millimetres cubed), the beta weights in V1 induced by TMS over the perilesional V1 area and the sum of the weighted ipsilesional V1–MT tracts. The backward regression model was significant [$F(2,9) = 8.7$, $P = 0.013$] and explained a relevant amount of the variance ($R^2 = 0.72$). The beta weights in V1 and the summed weights of the V1–MT tracts were retained as significant predictors [V1 beta weight: $t(9) = -3.1$, $P = 0.02$; sum: $t(9) = -3.3$, $P = 0.02$]. Importantly, the two predictors were not correlated with each other ($r = 0.29$, $P = 0.41$). The lesion size did not contribute to behavioural changes. Figure 5B illustrates the relationship between the change in NDR thresholds and V1 beta weights (left) or the summed weights of the tracts (right). Note that none of the demographical data (age and time since stroke) were correlated with visual improvements (all $P > 0.05$).

Discussion

Although non-invasive brain stimulation has been investigated widely in stroke patients for the recovery of motor functions, only a few clinical studies have applied brain stimulation to patients in conjunction with visual training.[62,63] Using conventional transcranial direct current stimulation (tDCS),[64-71] transcranial alternating current stimulation (tACS),[72] high frequency transcranial random noise stimulation[62] or repetitive transcranial magnetic stimulation[73] of the visual cortex, most of these studies showed promising results (but see Räty *et al.*[74]). Here, we developed a new interventional strategy based on co-entrainment of inter-regional oscillatory activity to synchronize feedforward oscillatory interactions using multifocal, pathway-specific, physiology-inspired cf-tACS to reduce visual impairment after an occipital stroke. The improvements in motion detection thresholds and in kinetic perimetry were observed in a relevant part of our cohort, which transferred to everyday life experiences. For instance, Patient P206 reported being 'able to see the right arm of his wife when seated on the passenger seat, when she is driving. This was impossible before the protocol'. This novel, physiology-inspired approach pairs brain stimulation with a motion training programme recognized as promising in patients with chronic cortically induced blindness, but which is intense to administer and requires lengthy treatment (several months) in order to elicit substantial benefits.[15,16,20] It builds on the recent evidence suggesting that deficits of vision secondary to a stroke might be caused by not only the primary focal tissue damage, but also by a change in inter-regional communication or functional synchronization in underlying brain networks.[75,76] Based on this pathophysiological concept, we investigated the effect of promoting forward (using forward cf-tACS: α-tACS over V1 and γ-tACS over MT) versus backward information flow (using backward cf-tACS as the control condition: γ-tACS over V1 and α-tACS over MT) on motion discrimination learning and visual field recovery.

Pathway and directed effects of cross-frequency tACS

The proposed physiology-inspired cf-tACS protocol is based on the extensive literature of animal model, human and computational modelling studies demonstrating that alpha-modulated gamma oscillations affect the probability of neurons in the visual system to respond to an incoming stimulus.[31,32,77,78] In an interareal regional framework, the neuronal population that mediates alpha oscillations projects onto the population oscillating at a gamma frequency, producing an efficient interareal communication channel in the visual system.[78-80] In the present study, forward cf-tACS, which we postulated to enhance feedforward information flow, resulted in enhanced motion discrimination and integration learning in comparison to backward cf-tACS in stroke patients with occipital cortex damage (for a schematic summary of results, see Fig. 6).

In line with the idea that forward cf-tACS could act by restoring optimal interareal oscillatory interactions, the EEG-based PAC between V1 and MT showed phasic modulations during motion processing in both directions. More precisely, the bottom-up V1 α_{phase}–MT γ_{amp} coupling significantly increased after forward cf-tACS during the first 100 ms of motion processing, suggesting enhanced early feedforward inputs to MT, followed by a significant decrease, probably preventing the system from saturating.[81] PAC has been proposed to coordinate neural processing by gating local neural activity, reflected in high-frequency oscillations, through a temporal window of a low-frequency oscillation.[80] A previous local field potential study investigating interareal PAC mechanisms suggested that high-gamma oscillations reflect population spiking, i.e. the output activity of a neuronal ensemble, whereas low-frequency oscillations (in our case, in alpha) reflect somatic/dendritic processing, hence the input activity of a neuronal ensemble.[36] By connecting the output of a driver with the input of a receiver network, this mechanism ensures pathway and direction-dependent communication, which is optimized in the present study for motion-related signal processing, increasing motion decoding. A possible scenario involves coordinated activity of excitatory and inhibitory neuronal populations in perilesional V1 influencing postsynaptic potentials at gamma frequencies in neurons projecting to MT[36] either directly or indirectly via V2 or V3.[82,83] This scenario is supported further by our fMRI results showing increased activity in perilesional V1 and in MT after forward cf-tACS, potentially capturing enhanced low-frequency coupling between MT and V1 44, which would match with the expected enhanced feedforward inputs induced by forward cf-tACS. The EEG data also showed an increase in the opposite MT α_{phase}–V1 γ_{amp} PAC during the late time window of motion processing (>300 ms after stimulus onset), as additional top-down modulations after forward cf-tACS. Overall, our results suggest that forward cf-tACS is likely to reactivate dynamical patterns of bi-directional V1–MT coupling, acting on the full feedforward–feedback motion processing loop.

Interestingly, our results showed that training on a motion direction discrimination task (irrespective of the cf-tACS condition) was associated with increased BOLD activity in the ipsilesional V1. This is in line with past studies showing that visual training in cortically blind patients results in an enlargement of population receptive fields in the perilesional V1, and increases blind-field coverage in these patients.[84] Previous visual relearning studies suggest that patients might require several dozen practice sessions over weeks and months before showing meaningful improvements in visual field recovery.[16,19,60] In the present study, 11 of the 15 patients in the forward cf-tACS condition showed meaningful improvements of direction range thresholds after only six sessions. This suggests that the rate of improvement in NDR thresholds in our study might be several times faster than the ones reported in previous studies using comparable tasks. Future studies should investigate whether increasing the training regimen and tACS dose would lead to better results, especially given that visual relearning might have a protective effect against trans-synaptic retrograde degeneration occurring after a stroke.[85] In a similar attempt to speed up

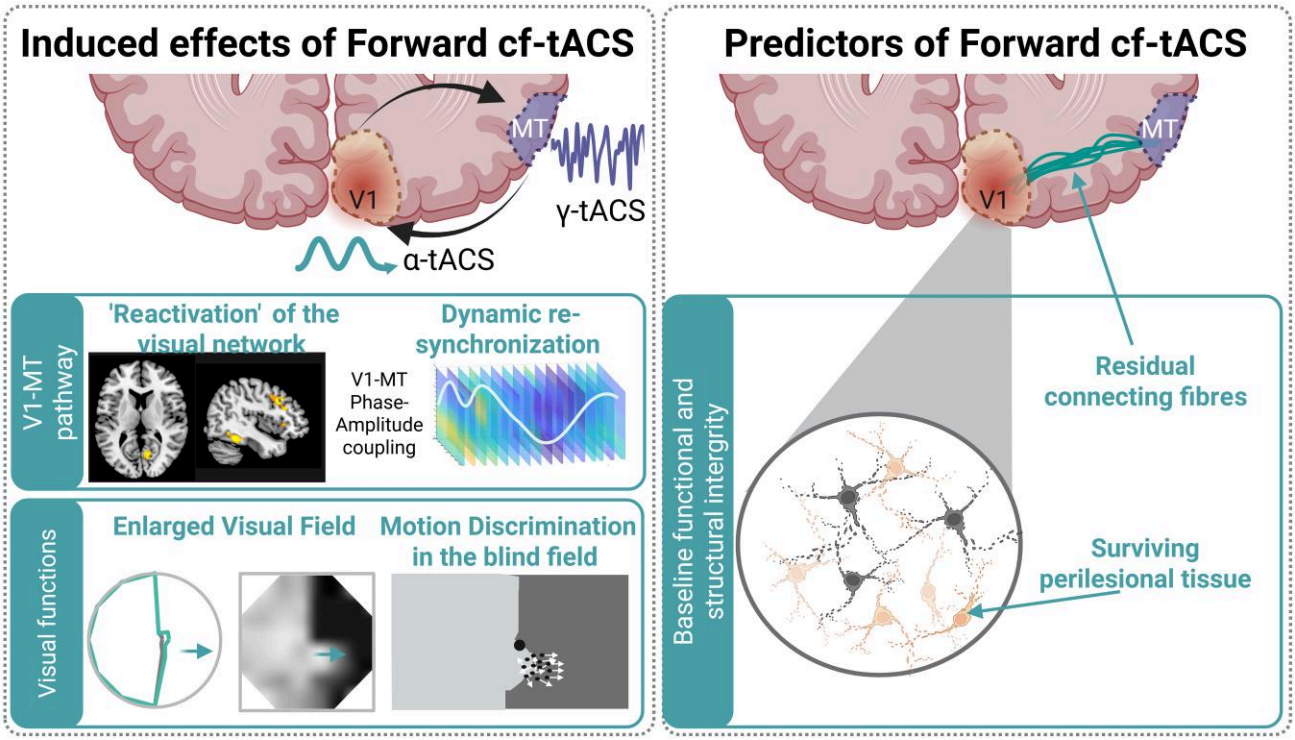

Figure 6 Graphical summary of the results. The clinical, behavioural and neuronal changes induced by the forward cf-tACS intervention (*left panel*) and the structural and functional variables that were associated with visual improvements (*right*). cf-tACS = cross-frequency transcranial alternating current stimulation.

relearning of visual motion discrimination learning in blind fields of homonymous hemianopia patients, Herpich *et al.*[62] administered visual training coupled with transcranial random noise stimulation. The results showed comparable extra-learning than with forward cf-tACS, but in the present study, we provide, for the first time, encouraging evidence that the extra-learning is coupled with enhanced visual field recovery in comparison to training alone or to backward cf-tACS, and we provide a unique set of multimodal neurophysiological markers of the intervention. Forward cf-tACS might also allow patients to regain a similar amount of visual field as reported by these past studies after months of training, in a much shorter period of time. Another important aspect to consider when referring to these earlier studies is the different study designs. Previous studies were home based, enhancing patient compliance but with limited control on the exact set-up (eye movements, level of attention etc.). In our proof-of-concept study, patients were training every day in the laboratory, with continuous eye tracking monitoring and feedback from a researcher.

Static perimetry is currently the most commonly used type of perimetry to assess visual field maps. Our results revealed a mean increase of 62.9°^{2} (for forward cf-tACS) and 65.5°^{2} (for backward cf-tACS). These values are within the range of results obtained after months of training sessions reported in home-based studies (from +~45°^{2}[19] to +~100°^{2}[15,16,64,75,76,86]) after ≥4 months of training. Improved motion direction discrimination and V1–MT oscillatory interactions when training was combined with forward cf-tACS also translated into an enlargement of visual field borders assessed with kinetic perimetry, in comparison to backward cf-tACS. Interestingly, in most of the patients (see Supplementary Fig. 1), the improvements were localized in the area that had been stimulated visually during the training protocol, confirming the retinotopic specificity of the training-induced improvements.[16,60] Hence, future studies should incorporate complementary ways of assessing visual field recovery, such as kinetic perimetry, potentially more sensitive to subtle changes.

Extending the capacity to detect motion in the blind field definitively has a positive and practical impact in patients' lives, as acknowledged by the positive comments from our patients. However, the limitations associated with this study should be considered. First, although similar to the sample sizes found in comparable studies,[14,62,84] the small number of patients in this study prevents the results from being generalized broadly. Second, we did not measure long-term effects of the protocol. Therefore, it is unknown whether patients retain their visual improvements months after the end of the intervention. Third, although we controlled for the directionality of the oscillatory interactions, we did not include a direct comparison to conventional transcranial direct current stimulation or tACS nor a sham tACS condition. Future studies with a pure sham intervention would help to disentangle the improvements explained by the visual training alone, by the tACS intervention alone or by the interaction between the two. Finally, future studies should also include objective measurements of the clinically meaningful effects of the intervention.

Predictive values of residual V1 reactivity and V1–MT structural integrity

The multimodal evaluation battery performed before and after the intervention aimed to evaluate predictors of forward cf-tACS effects. Based on prior literature,[84] our initial hypothesis was that the residual V1 neurons spared by the lesion are crucial for visual recovery. To probe causally the level of residual functions of perilesional V1 neurons in the present study, we used the unique opportunity of TMS–fMRI to measure the local response to TMS in the perilesional area before the intervention. We found that

TMS-evoked activity was predictive of the changes induced by training + forward cf-tACS in direction range thresholds in the blind field (there was no such association with training + backward cf-tACS), suggesting that the more functional surviving cortical tissue, the more likely it is that a patient will benefit from forward cf-tACS. Conversely to tACS, TMS depolarizes neurons in the stimulated region and results in localized neural activity that drives metabolic demand, indirectly measured with BOLD signal change. Although it is impossible to disentangle the type of neuronal activity underlying BOLD signal change, it offers insights into the function of the targeted brain area and its interactions with other regions. Our group results showed BOLD activity in the stimulated ipsilesional V1 cortex, near to the lesion. This could indicate that residual pathways or spared neurons in the perilesional area might still be functional and connected with anatomically but also functionally relevant areas. Another strong predictor of forward cf-tACS effects was the number of structural fibres connecting V1 to MT. The relationship between structural markers and brain stimulation effects has been shown repeatedly in various contexts and networks.[86-89] Again, this finding provides another piece of evidence for target engagement, with both training and forward cf-tACS relying strongly on the cortical motion pathway for their effects. Notably, those two independent variables need to be considered together to explain a sufficient amount of variance in the response to forward cf-tACS.

Conclusion

The results provide first proof-of-concept evidence that pathway-specific, physiology-inspired tACS might be a novel treatment opportunity to boost post-stroke visual field recovery. The intervention relies on the hierarchical oscillatory interactions between visual cortical areas, which can be supported or restored with this physiologically inspired protocol. The unique set of multimodal measurements confirmed the relevance of these oscillatory channels for visual learning in patients and showed reactivation of the ipsilesional V1–MT pathway.

Data availability

The datasets used for this study are available from the corresponding author on reasonable request.

Acknowledgements

We would like to thank the EEG and neuromodulation facilities of the Human Neuroscience Platform of the Foundation Campus Biotech Geneva, for technical advice, and the Brain & Behavior Laboratory (BBL) facilities at the Centre Medical Universitaire (CMU) of Geneva.

Funding

Funding was obtained from the Defitech Foundation (to F.C.H.), Bertarelli Foundation (Catalyst BC77O7 to F.C.H. and E.R.), by the Swiss National Science Foundation (SNSF) (PRIMA PR00P3_179867 to E.R.).

Competing interests

The authors declare that they have no competing interests.

Supplementary material

Supplementary material is available at Brain online.

References

1. Hepworth L, Rowe F, Walker M, et al. Post-stroke visual impairment: A systematic literature review of types and recovery of visual conditions. *Ophthalmol Res Int J*. 2016;5:1–43.
2. Rowe FJ, Wright D, Brand D, et al. A prospective profile of visual field loss following stroke: Prevalence, type, rehabilitation, and outcome. *BioMed Res Int*. 2013;2013:719096.
3. Liu NJV, Galetta SL. Retrochiasmal disorders. *Neuro-ophthalmology: Diagnosis and management*. W.B. Saunders; 2001:296.
4. Peli E, Apfelbaum H, Berson EL, Goldstein RB. The risk of pedestrian collisions with peripheral visual field loss. *J Vis*. 2016;16:5.
5. Ungewiss J, Kübler T, Sippel K, et al. Agreement of driving simulator and on-road driving performance in patients with binocular visual field loss. *Graefes Arch Clin Exp Ophthalmol*. 2018;256:2429–2435.
6. Chen CS, Lee AW, Clarke G, et al. Vision-related quality of life in patients with complete homonymous hemianopia post stroke. *Top Stroke Rehabil*. 2009;16:445–453.
7. Papageorgiou E, Hardiess G, Schaeffel F, et al. Assessment of vision-related quality of life in patients with homonymous visual field defects. *Graefes Arch Clin Exp Ophthalmol*. 2007;245:1749–1758.
8. Bowers AR, Keeney K, Peli E. Randomized crossover clinical trial of real and sham peripheral prism glasses for hemianopia. *JAMA Ophthalmol*. 2014;132:214–222.
9. O'Neill EC, Connell PP, O'Connor JC, Brady J, Reid I, Logan P. Prism therapy and visual rehabilitation in homonymous visual field loss. *Optometry Vis Sci*. 2011;88:263–268.
10. Sahraie A, Cederblad AMH, Kenkel S, Romano JG. Efficacy and predictors of recovery of function after eye movement training in 296 hemianopic patients. *Cortex*. 2020;125:149–160.
11. And KT, Kolmel HW. Patterns of recovery from homonymous hemianopia subsequent to infarction in the distribution of the posterior cerebral artery. *Neuro-Ophthalmol*. 1991;11:33–39.
12. Gray CS, French JM, Bates D, Cartlidge NEF, Venables GS, James OFW. Recovery of visual fields in acute stroke: Homonymous hemianopia associated with adverse prognosis. *Age Ageing*. 1989;18:419–421.
13. Zhang X, Kedar S, Lynn MJ, Newman NJ, Biousse V. Natural history of homonymous hemianopia. *Neurology*. 2006;66:901–905.
14. Cavanaugh MR, Zhang R, Melnick MD, et al. Visual recovery in cortical blindness is limited by high internal noise. *J Vis*. 2015;15:9.
15. Cavanaugh MR, Huxlin KR. Visual discrimination training improves Humphrey perimetry in chronic cortically induced blindness. *Neurology*. 2017;88:1856–1864.
16. Huxlin KR, Martin T, Kelly K, et al. Perceptual relearning of complex visual motion after V1 damage in humans. *J Neurosci*. 2009;29:3981–3991.
17. Raninen A, Vanni S, Hyvärinen L, Näsänen R. Temporal sensitivity in a hemianopic visual field can be improved by long-term training using flicker stimulation. *J Neurol Neurosurg Psychiatry*. 2007;78:66–73.
18. Sahraie A, Trevethan CT, MacLeod MJ, Murray AD, Olson JA, Weiskrantz L. Increased sensitivity after repeated stimulation of residual spatial channels in blindsight. *Proc Natl Acad Sci U S A*. 2006;103:14971–14976.
19. Saionz EL, Tadin D, Melnick MD, Huxlin KR. Functional preservation and enhanced capacity for visual restoration in subacute occipital stroke. *Brain*. 2020;143:1857–1872.

20. Das A, Tadin D, Huxlin KR. Beyond blindsight: Properties of visual relearning in cortically blind fields. *J Neurosci*. 2014;34:11652–11664.
21. Melnick MD, Tadin D, Huxlin KR. Relearning to see in cortical blindness. *Neurosci Rev J Bringing Neurobiol Neurol Psychiatry*. 2016;22:199–212.
22. Buzsáki G, Anastassiou CA, Koch C. The origin of extracellular fields and currents—EEG, ECoG, LFP and spikes. *Nat Rev Neurosci*. 2012;13:407–420.
23. Tort ABL, Komorowski RW, Manns JR, Kopell NJ, Eichenbaum H. Theta–gamma coupling increases during the learning of item–context associations. *Proc Natl Acad Sci U S A*. 2009;106:20942–20947.
24. Axmacher N, Henseler MM, Jensen O, Weinreich I, Elger CE, Fell J. Cross-frequency coupling supports multi-item working memory in the human hippocampus. *Proc Natl Acad Sci U S A*. 2010;107:3228–3233.
25. de Hemptinne C, Ryapolova-Webb ES, Air EL, et al. Exaggerated phase–amplitude coupling in the primary motor cortex in Parkinson disease. *Proc Natl Acad Sci U S A*. 2013;110:4780–4785.
26. Khamechian MB, Daliri MR, Treue S, Esghaei M. Coupled oscillations orchestrate selective information transmission in visual cortex. *PNAS Nexus*. 2024;3:pgae288.
27. Esghaei M, Daliri MR, Treue S. Attention decreases phase-amplitude coupling, enhancing stimulus discriminability in cortical area MT. *Front Neural Circuits*. 2015;9:82.
28. Esghaei M, Treue S, Vidyasagar TR. Dynamic coupling of oscillatory neural activity and its roles in visual attention. *Trends Neurosci*. 2022;45:323–335.
29. Yang X, Fiebelkorn IC, Jensen O, Knight RT, Kastner S. Differential neural mechanisms underlie cortical gating of visual spatial attention mediated by alpha-band oscillations. *Proc Natl Acad Sci U S A*. 2024;121:e2313304121.
30. von Stein A, Chiang C, König P. Top-down processing mediated by interareal synchronization. *Proc Natl Acad Sci U S A*. 2000;97:14748–14753.
31. van Kerkoerle T, Self MW, Dagnino B, et al. Alpha and gamma oscillations characterize feedback and feedforward processing in monkey visual cortex. *Proc Natl Acad Sci U S A*. 2014;111:14332–14341.
32. Bonnefond M, Jensen O. Gamma activity coupled to alpha phase as a mechanism for top-down controlled gating. *PLoS One*. 2015;10:e0128667.
33. Spaak E, Bonnefond M, Maier A, Leopold DA, Jensen O. Layer-specific entrainment of gamma-band neural activity by the alpha rhythm in monkey visual cortex. *Curr Biol*. 2012;22:2313–2318.
34. Voytek B, Canolty R, Shestyuk A, Crone N, Parvizi J, Knight R. Shifts in gamma phase–amplitude coupling frequency from theta to alpha over posterior cortex during visual tasks. *Front Hum Neurosci*. 2010;4:191.
35. Bevilacqua M, Feroldi S, Windel F, et al. Single session cross-frequency bifocal tACS modulates visual motion network activity in young healthy population and stroke patients. *Brain Stimul*. 2024;17:660–667.
36. Nandi B, Swiatek P, Kocsis B, Ding M. Inferring the direction of rhythmic neural transmission via inter-regional phase-amplitude coupling (ir-PAC). *Sci Rep*. 2019;9:6933.
37. Salamanca-Giron RF, Raffin E, Zandvliet SB, et al. Enhancing visual motion discrimination by desynchronizing bifocal oscillatory activity. *NeuroImage*. 2021;240:118299.
38. Barton JJS, Benatar M. Goldmann perimetry. In: Barton JJS, Benatar M, eds. *Field of vision: A manual and atlas of perimetry*. Humana Press; 2003:31–44.
39. Weijland A, Fankhauser F, Bebie H, Flammer J. Automated perimetry: visual field digest. Accessed 28 November 2023. https://www.semanticscholar.org/paper/Automated-perimetry-%3A-visual-field-digest-Weijland-Fankhauser/300c780d1fb2064f5f6c86b54c98423ac4c0cf82
40. Ma X, Tang L, Chen X, Zeng L. Periphery kinetic perimetry: Clinically feasible to complement central static perimetry. *BMC Ophthalmol*. 2021;21:343.
41. Delorme A, Makeig S. EEGLAB: An open source toolbox for analysis of single-trial EEG dynamics including independent component analysis. *J Neurosci Methods*. 2004;134:9–21.
42. Tadel F, Baillet S, Mosher JC, Pantazis D, Leahy RM. Brainstorm: A user-friendly application for MEG/EEG analysis. *Comput Intell Neurosci*. 2011;2011:879716.
43. Reuter M, Schmansky NJ, Rosas HD, Fischl B. Within-subject template estimation for unbiased longitudinal image analysis. *NeuroImage*. 2012;61:1402–1418.
44. Gramfort A, Papadopoulo T, Olivi E, Clerc M. OpenMEEG: Opensource software for quasistatic bioelectromagnetics. *Biomed Eng Online*. 2010;9:45.
45. Canolty RT, Edwards E, Dalal SS, et al. High gamma power is phase-locked to theta oscillations in human neocortex. *Science*. 2006;313:1626–1628.
46. Martinez-Cancino R, Heng J, Delorme A, Kreutz-Delgado K, Sotero RC, Makeig S. Measuring transient phase-amplitude coupling using local mutual information. *NeuroImage*. 2019;185:361–378.
47. Ashburner J, Friston KJ. Unified segmentation. *NeuroImage*. 2005;26:839–851.
48. Ruff CC, Driver J, Bestmann S. Combining TMS and fMRI. *Cortex J Devoted Study Nerv Syst Behav*. 2009;45:1043–1049.
49. Jenkinson M, Beckmann CF, Behrens TEJ, Woolrich MW, Smith SM. FSL. *NeuroImage*. 2012;62:782–790.
50. Tournier JD, Smith R, Raffelt D, et al. MRtrix3: A fast, flexible and open software framework for medical image processing and visualisation. *NeuroImage*. 2019;202:116137.
51. Veraart J, Novikov DS, Christiaens D, Ades-Aron B, Sijbers J, Fieremans E. Denoising of diffusion MRI using random matrix theory. *NeuroImage*. 2016;142:394–406.
52. Andersson JLR, Skare S, Ashburner J. How to correct susceptibility distortions in spin-echo echo-planar images: Application to diffusion tensor imaging. *NeuroImage*. 2003;20:870–888.
53. Andersson JLR, Sotiropoulos SN. An integrated approach to correction for off-resonance effects and subject movement in diffusion MR imaging. *NeuroImage*. 2016;125:1063–1078.
54. Smith SM, Jenkinson M, Woolrich MW, et al. Advances in functional and structural MR image analysis and implementation as FSL. *NeuroImage*. 2004;23(Suppl 1):S208–S219.
55. Zhang Y, Brady M, Smith S. Segmentation of brain MR images through a hidden Markov random field model and the expectation-maximization algorithm. *IEEE Trans Med Imaging*. 2001;20:45–57.
56. Avants BB, Tustison N, Johnson H. Advanced Normalization Tools (ANTS). *Insight J*. 2008;1:1–35.
57. Tournier JD. Diffusion MRI in the brain—Theory and concepts. *Prog Nucl Magn Reson Spectrosc*. 2019;112–113:1–16.
58. Smith RE, Tournier JD, Calamante F, Connelly A. SIFT2: Enabling dense quantitative assessment of brain white matter connectivity using streamlines tractography. *NeuroImage*. 2015;119:338–351.
59. Yendiki A, Panneck P, Srinivasan P, et al. Automated probabilistic reconstruction of white-matter pathways in health and disease using an atlas of the underlying anatomy. *Front Neuroinform*. 2011;5:23.

60. Cavanaugh MR, Barbot A, Carrasco M, Huxlin KR. Feature-based attention potentiates recovery of fine direction discrimination in cortically blind patients. *Neuropsychologia*. 2019;128:315–324.
61. Bevilacqua M, Feroldi S, Windel F, et al. Single session cross-frequency bifocal tacs modulates visual motion network activity in young healthy and stroke patients. *Brain Stimul*. 2024;17:660–667.
62. Herpich F, Melnick MD, Agosta S, Huxlin KR, Tadin D, Battelli L. Boosting learning efficacy with noninvasive brain stimulation in intact and brain-damaged humans. *J Neurosci*. 2019;39:5551–5561.
63. Battaglini L, Di Ponzio M, Ghiani A, Mena F, Santacesaria P, Casco C. Vision recovery with perceptual learning and non-invasive brain stimulation: Experimental set-ups and recent results, a review of the literature. *Restor Neurol Neurosci*. 2022;40:137–168.
64. Matteo BM, Viganò B, Cerri CG, Meroni R, Cornaggia CM, Perin C. Transcranial direct current stimulation (tDCS) combined with blindsight rehabilitation for the treatment of homonymous hemianopia: A report of two-cases. *J Phys Ther Sci*. 2017;29:1700–1705.
65. Plow EB, Obretenova SN, Halko MA, et al. Combining visual rehabilitative training and noninvasive brain stimulation to enhance visual function in patients with hemianopia: A comparative case study. *PM&R*. 2011;3:825–835.
66. Plow EB, Obretenova SN, Fregni F, Pascual-Leone A, Merabet LB. Comparison of visual field training for hemianopia with active versus sham transcranial direct cortical stimulation. *Neurorehabil Neural Repair*. 2012;26:616–626.
67. Bakulin IS, Сергеевич БИ, Lagoda DY, et al. Transcranial direct current stimulation in poststroke hemianopia. *Ann Clin Exp Neurol*. 2020;14:5–14.
68. Lian Y, Cheng X, Chen Q, et al. Case report: Beneficial effects of visual cortex tDCS stimulation combined with visual training in patients with visual field defects. *Front Neurol*. 2024;15:1344348.
69. Larcombe SJ, Kulyomina Y, Antonova N, et al. Visual training in hemianopia alters neural activity in the absence of behavioural improvement: A pilot study. *Ophthalmic Physiol Opt J Br Coll Ophthalmic Opt Optom*. 2018;38:538–549.
70. Alber R, Moser H, Gall C, Sabel BA. Combined transcranial direct current stimulation and vision restoration training in subacute stroke rehabilitation: A pilot study. *PM&R*. 2017;9:787–794.
71. Halko M, Datta A, Plow E, Scaturro J, Bikson M, Merabet L. Neuroplastic changes following rehabilitative training correlate with regional electrical field induced with tDCS. *NeuroImage*. 2011;57:885–891.
72. Toba MN, Potet A, Gobatto C, et al. Transcranial alternating current stimulation (tACS) for the rehabilitation of homonymous hemianopia following unilateral stroke: Current evidence from an ongoing pilot study. *Brain Stimul Basic Transl Clin Res Neuromodulation*. 2023;16:251–252.
73. Tiksnadi A, Tunjungsari D, Tannika A, et al. Alteration of post stroke visual field defects after repetitive transcranial magnetic stimulation. *Brain Stimul Basic Transl Clin Res Neuromodulation*. 2023;16:318.
74. Räty S, Borrmann C, Granata G, et al. Non-invasive electrical brain stimulation for vision restoration after stroke: An exploratory randomized trial (REVIS). *Restor Neurol Neurosci*. 2021;39:221–235.
75. Raffin E, Salamanca-Giron RF, Hummel FC. Perspectives: Hemianopia—Toward novel treatment options based on oscillatory activity? *Neurorehabil Neural Repair*. 2020;34:13–25.
76. Siegel M, Donner TH, Oostenveld R, Fries P, Engel AK. Neuronal synchronization along the dorsal visual pathway reflects the focus of spatial attention. *Neuron*. 2008;60:709–719.
77. Bahramisharif A, van Gerven MAJ, Aarnoutse EJ, et al. Propagating neocortical gamma bursts are coordinated by traveling alpha waves. *J Neurosci*. 2013;33:18849–18854.
78. Osipova D, Hermes D, Jensen O. Gamma power is phase-locked to posterior alpha activity. *PLoS One*. 2008;3:e3990.
79. Bonnefond M, Kastner S, Jensen O. Communication between brain areas based on nested oscillations. *eNeuro*. 2017;4:1–14.
80. Canolty RT, Knight RT. The functional role of cross-frequency coupling. *Trends Cogn Sci*. 2010;14:506–515.
81. Chacko RV, Kim B, Jung SW, et al. Distinct phase-amplitude couplings distinguish cognitive processes in human attention. *NeuroImage*. 2018;175:111–121.
82. Nassi JJ, Callaway EM. Specialized circuits from primary visual cortex to V2 and area MT. *Neuron*. 2007;55:799–808.
83. Shipp S, Zeki S. Segregation of pathways leading from area V2 to areas V4 and V5 of macaque monkey visual cortex. *Nature*. 1985;315:322–324.
84. Barbot A, Das A, Melnick MD, et al. Spared perilesional V1 activity underlies training-induced recovery of luminance detection sensitivity in cortically-blind patients. *Nat Commun*. 2021;12:6102.
85. Fahrenthold BK, Cavanaugh MR, Tamhankar M, et al. Training in cortically blinded fields appears to confer patient-specific benefit against retinal thinning. *Invest Ophthalmol Vis Sci*. 2024;65(4):1–29.
86. Kearney-Ramos T, Lench D, Hoffman M, Correia B, Dowdle L, Hanlon C. Gray and white matter integrity influence TMS signal propagation: A multimodal evaluation in cocaine-dependent individuals. *Sci Rep*. 2018;8:3253.
87. Khan A, Mosbacher JA, Vogel SE, et al. Modulation of resting-state networks following repetitive transcranial alternating current stimulation of the dorsolateral prefrontal cortex. *Brain Struct Funct*. 2023;228:1643–1655.
88. Momi D, Ozdemir RA, Tadayon E, et al. Network-level macroscale structural connectivity predicts propagation of transcranial magnetic stimulation. *NeuroImage*. 2021;229:117698.
89. Muthuraman M, Deuschl G, Koirala N, Riedel C, Volkmann J, Groppa S. Effects of DBS in parkinsonian patients depend on the structural integrity of frontal cortex. *Sci Rep*. 2017;7:43571.

Supplementary materials

Transcranial Magnetic Stimulation combined with functional Magnetic Resonance Imaging

To probe the functional state of the perilesional area and investigate how stimulation of the perilesional area propagates to the rest of the brain, we used online TMS-fMRI coupling [1]. For this purpose, two dedicated coil arrays were used [2]. This setup consisted of an ultra-slim 7-channel receive-only coil array, which was placed between the subject's head and the TMS coil (MRi-B91, MagVenture, Farum, Denmark) and connected to a MagPro XP stimulator (MagVenture, Farum, Denmark). A second, receive-only MR coil was positioned over Cz in the EEG 10-20 system to allow a full coverage of the participant's brain.

An event-related design was used to map the effect of TMS bursts composed of three pulses at alpha (10Hz) frequency. Three conditions were pseudorandomized and counterbalanced across the run: high-intensity TMS (*HighTMS)*, low-intensity TMS *(LowTMS)* and no TMS *(noTMS)*. There were 25 repetitions of each condition, with an inter-trial interval (ITI) of 6 seconds (covering 3 repetition times). The TMS intensity was set to ≈ 80% [range: 75 to 90%] maximal stimulator output (MSO) for the *HighTMS* condition, and ≈38 % [35 to 43%] MSO for the *LowTMS* condition. Intensity was individually adjusted prior to the measurement to ensure phosphene sub-threshold stimulation and progressively increased until patients reported discomfort. The intensity was then chosen to achieve a reliable BOLD signal while preserving participant comfort. Participants were asked to look at a fixation cross throughout the acquisition, displayed in the middle of a 44cm x 27cm LCD monitor at a 2.5m distance, via a mirror mounted on the head coil or on a frame on top of the TMS-fMRI setup. The duration

of the *Rest TMS* sequence was 9 minutes. The TMS coil was individually placed to target perilesional cortex using oil capsules placed on the TMS-MRI coil casing to monitor the coil position visible on a T2 image (see Supplementary Figure S4B for the TMS targeting of all patients).

The *TMS-fMRI* sequences were acquired with a GE-EPI sequence using the same parameters: 40 axial slices, slice thickness = 2.2 mm, in-plane resolution = 2.2 mm, TR = 2000 ms, TE = 30 ms, FOV = 242 mm, flip angle = 67°, GRAPPA = 2, Multiband Factor (MB) = 2. A gap was introduced between consecutive EPI volumes in order to guarantee artefact free MR images after TMS stimulation [3]. A single repetition time (TR=2000 ms) was therefore composed of 40 slices acquired during 1430 ms followed by a gap of 570 ms before the next volume acquisition. The synchronization of the TMS pulse was carried out with an in-house script using Matlab (R2019).

Static field mapping was also performed with the TMS-MRI coils using the same double-echo spoiled gradient echo sequence (TR = 652 ms, TE = 4.92 and 7.38 ms, slice thickness: 2.2 mm, in-plane resolution = 2.2 mm, flip angle = 60°) that generates two magnitude images and one image representing the phase difference between the two echoes.

The same pre-processing steps than the ones described above were applied to the fMRI data except for two additional co-registration steps. A first co-registration was performed between the mean realigned and slice-timing-corrected image and the SSFP sequence acquired with the same MR coil (and thus the same spatial coverage). The resulting, co-registered image was once more co-registered to the SSFP sequence acquired with the MR coil integrated into the scanner (i.e., the body coil, thus preserving the contrast). The latter could then be easily co-registered to the high resolution T1-weighted image acquired with the

64-channel head coil that covered the whole brain, and later transformed into standard MNI space using a segmentation-based normalization approach [4].

Univariate analyses were performed on the fMRI data. We defined a design matrix comprising the three conditions (*HighTMS*, *LowTMS* and *noTMS*). T-contrasts for each TMS condition were established for all participants. In this study, we focused on the contrast *HighTMS* versus Low*TMS* using a paired-t-test at the group level. The statistical significance threshold was set to $p < 0.001$ uncorrected at the voxel level and to $p < 0.05$ at the cluster level after false-discovery rate (FDR) correction. To explore inter-individual variability, mean beta values were extracted from individual ipsilesional V1 clusters.

Table S1: Cluster information and MNI coordinates of the fMRI full factorial design analysis during motion discrimination.

Regions	**F values**	**Z max**	**Cluster extent**	**MNI coordinates (x;y;z)**
Time effect (F test)				
R Primary Visual Cortex	13.4	3.35	31	4;-76;-3
R Med. Pre-Frontal Ctx.	12.7	3.26	19	3;46;3
L IFG	11.7	3.39	17	-29;46;28
Interaction Time X tACS cond.				
R MT	21.4	4.24	309	52;-56;-14
L Frontal Eye Field	17.56	3.85	44	46;22;34
R Frontal Eye Field	12.68	3.26	12	-38 ;12 ;46
R Prefrontal Ctx.	14.3	3.47	12	42 ;48 ;-8

Figure S1

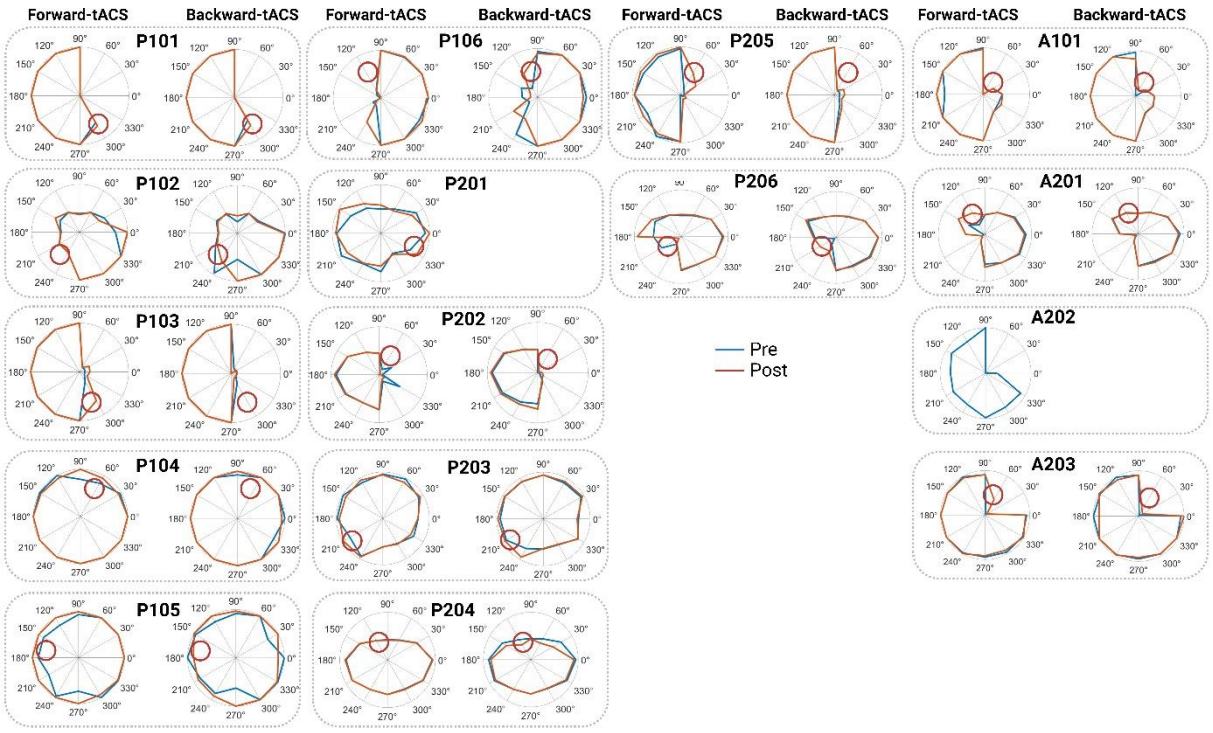

Individual composite kinetic visual field maps before and after the interventions. *Kinetic visual field maps before (blue contours) and after (red contours) Forward cf-tACS (left panels) and backward cf-tACS (right panels) for all individual patients, with the individual location of the visual stimulus used during the visual training denoted by a red circle on each map.*

Figure S2

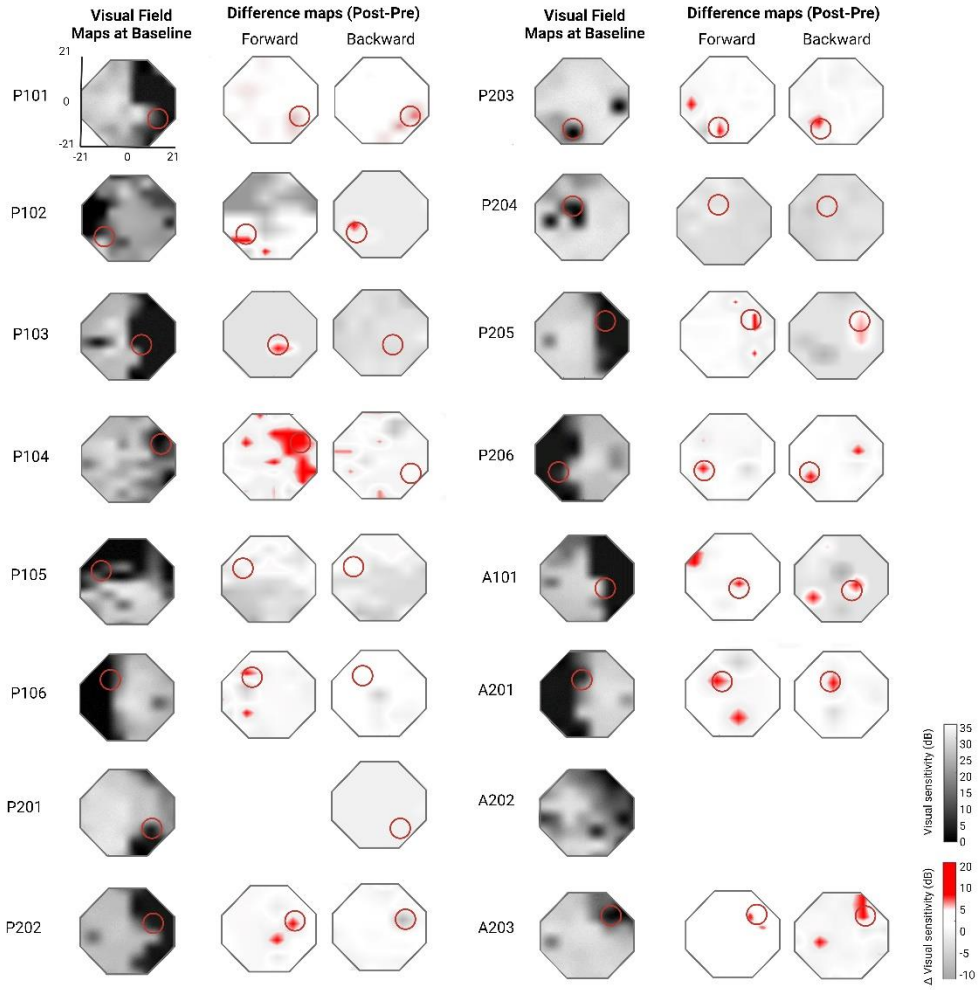

Individual composite static visual field maps before and after the interventions. *Baseline visual fields (left panels) and Post>Pre differences associated with Forward-tACS (Middle panels) and Backward-tACS (right panels). Changes were considered when visual sensitivity improved more than 6 dB. The red circle on each map symbolizes the location of the visual stimulus used for the CDDI training.*

Figure S3

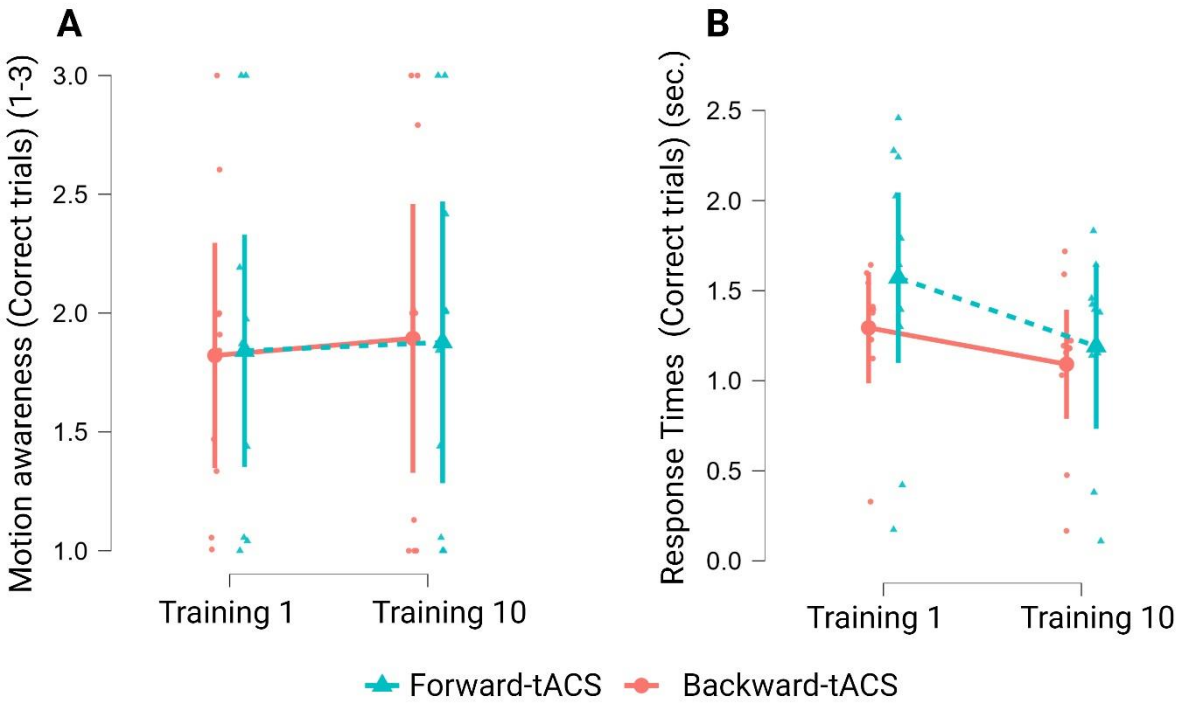

Motion awareness and response times. *Changes in motion awareness and response times after Forward-tACs (blue) and Backward-tACS (red). We also explored potential differences in motion awareness after the intervention, measured with a three items scale rating self-confidence on a trial-by-trial basis. eFigure 4A shows the difference in motion awareness between Training 1 and Training 10, on correct trials for the two tACS conditions. Subjective awareness of the stimulus did not significantly change between the first and the last sessions for both groups (Time effect: $F(1,11) = 0.7$, $p = 0.43$). Note that some patients reported a clear sensation of motion (the left-or rightward for the CDDI task) while some appeared to predominantly rely on non-conscious motion processing. Additionally, reaction times of correct trials showed a common decrease after training (significant Time effect: $F(1,20) = 13.1$, $p = 0.002$) but no Time by tACS condition interaction ($F(1,18) = 1.3$, $p = 0.27$).*

Figure S4

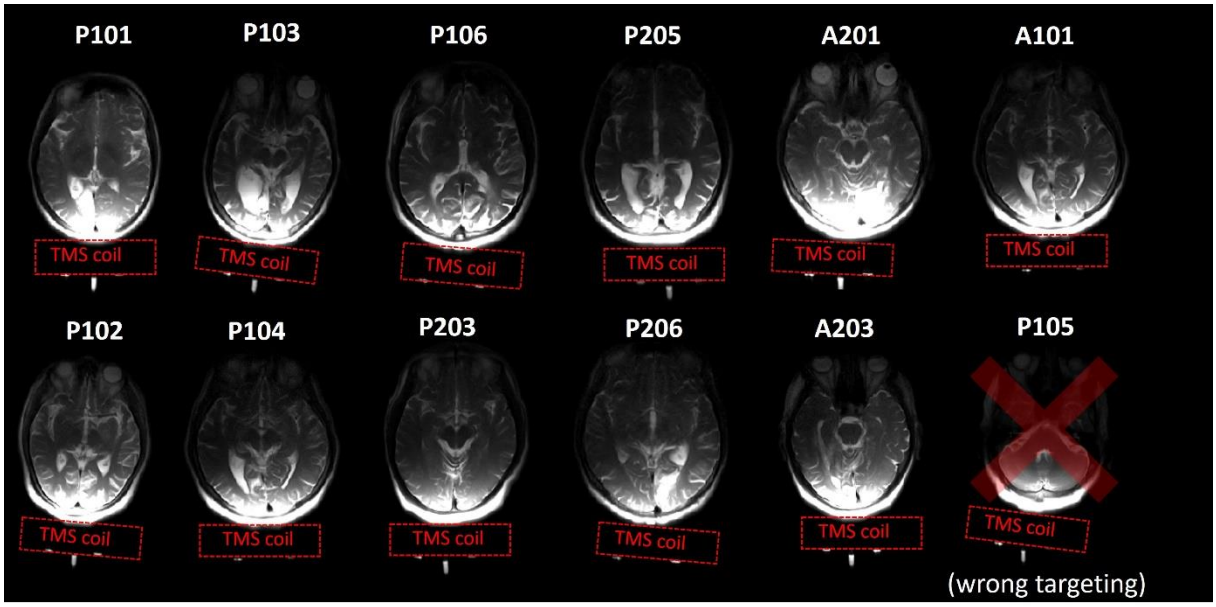

TMS-fMRI targeting in all patients. *Structural images based on t2 haste sequence displaying for all patients the TMS coil position targeting the perilesional area. Note that P105 was excluded from the analysis due to wrong targeting.*

Supplementary references

1. Ruff CC, Driver J, Bestmann S. Combining TMS and fMRI. *Cortex*. 2009;45(9):1043-1049. doi:10.1016/j.cortex.2008.10.012

2. Navarro de Lara LI, Tik M, Woletz M, et al. High-sensitivity TMS/fMRI of the Human Motor Cortex Using a Dedicated Multichannel MR Coil. *NeuroImage*. 2017;150:262-269. doi:10.1016/j.neuroimage.2017.02.062

3. Navarro de Lara LI, Windischberger C, Kuehne A, et al. A novel coil array for combined TMS/fMRI experiments at 3 T. *Magn Reson Med*. 2015;74(5):1492-1501. doi:10.1002/mrm.25535

4. Ashburner J, Friston KJ. Unified segmentation. *NeuroImage*. 2005;26(3):839-851. doi:10.1016/j.neuroimage.2005.02.018

Authors' contributions

ER and FCH designed the study. ER, MB, RFSG, SBZ, FW, PM acquired the data. ER analyzed the behavioral and fMRI data. EB and NR analyzed the structural MRI data. MB and SF analyzed the EEG data. PW and FW analyzed the clinical data. ER wrote the first version of the manuscript. All authors critically read and approved the final manuscript. KRH lab provided the codes and parameters for generating the training stimuli and some of the scripts for data analyses (i.e., for Weibull fitting).